

A Three-Dimensional Flow Focusing Microsecond Mixer for Dynamic Assessment of Nanoparticle Formation

Liguo Jiang and Shuhuai Yao

Abstract—This paper reports the design, fabrication, and characterization of a three-dimensional flow focusing microfluidic mixer. By hydrodynamically focusing the sample stream into a very confined jet in both vertical and horizontal directions, the mixer can achieve ultrafast mixing of reagents within $\sim 3 \pm 1 \mu\text{s}$. Such rapid mixing allows us to dynamically assess the formation of nanomaterial and study their assembly kinetics on microsecond timescale. Using the mixer, we investigated the formation of the hexaphenylsilole (HPS) nanoparticles. Compared to those formed by bulk nanoprecipitation, the HPS nanoparticles formed in the mixer have smaller size with narrower size distribution. We also kinetically resolved that the microsecond molecular self-assembly of HPS molecules displays two distinct steps. These results suggest that the formation of HPS nanoparticles follows the classical nucleation and growth theory.

Index Terms—3D flow focusing, nanoparticle, rapid mixing, self-assembly kinetics.

I. INTRODUCTION

FUNCTIONAL and bioactive nanoparticles are very promising for drug delivery, bioimaging, and sensor applications [1]–[3]. For instance, those biocompatible nanoparticles synthesized from aggregation-induced emission (AIE) materials [4] are promising for noninvasive long-term cell tracing [5]. In general, the synthesis of nanoparticles is based on molecular self-assembly [6]–[8]. For the nanoparticles to serve as effective imaging and/or therapy agents, the size of nanoparticles is a key factor in the biodistribution and clearance of the circulating system [9]. Therefore, synthesis of nanoparticles with controllable size and good uniformity are crucial in many biological applications. However, the conventional synthesis method by bulk nanoprecipitation, in which a small volume of stock sample solution is dropped into a larger volume of water and mixing of solutions by vortex, usually results in formed nanoparticles with wide size distribution, because the mixing of reagents by

vortex is slow and uncontrollable. This implies that rapid mixing is crucial for synthesis of nanoparticles with narrow size distribution.

Microfluidic mixing techniques with the ability of rapid and controllable mixing of reagents provide an alternative way for synthesis of nanoparticles [10], [11]. Particularly, the microfluidic mixing by hydrodynamic flow focusing (HFF) [12], in which the central stream is hydrodynamically focused by two side buffer streams at a cross junction under laminar flow condition, is a very attractive technique for nanomaterial synthesis, because it enables precise control of the convective-diffusive mixing of reagents and provides a homogeneous reaction environment after rapid mixing. Moreover, ultrafast mixing induced by HFF also facilitate the measurement of fast biochemical reaction kinetics [13], [14], including protein folding and molecular self-assembly. To achieve controllable synthesis of nanomaterials, the kinetic investigation of molecular self-assembly is indispensable. In addition, the time course of the reaction in the HFF system is converted into the spatial course along the focused jet. This allows us to follow and capture the kinetics of the nanoparticle formation along the trajectory of the focused jet. Further, the formed nanomaterials in the focused jet can be characterized by fluorescence microscopy, Raman scattering, or small angle X-ray scattering, etc.

In previous studies, the two-dimensional (2D) HFF system, in which the sample in the central stream is only focused in the lateral plane, may encounter several problems such as sticking of molecules on the channel surface walls due to the hydrophobic or electrostatic forces, and non-uniform mixing due to the parabolic velocity profile in the vertical plane. 3D HFF offers a superior solution that could resolve those problems encountered in the 2DHFF [15], [16]. For example, Rhee *et al.* [15] successfully fabricated a single-layer 3DHFF device for synthesizing of polymeric nanoparticles as drug carriers. A more recent work of Lu *et al.* [17] achieved a 3DHFF in a single layered, planar microfluidic device [18] to synthesize of polyplexes nanomaterial with small size and high transfection efficiency for drug delivery. In addition, with the ability to precisely position the flow stream in microchannels, 3DHFF were also applied to achieve hydrodynamically focus cells or particles as on-chip flow cytometer for high-throughput flow cytometry measurements [19]. Nevertheless, most of the 3DHFF devices were made in polydimethylsiloxane (PDMS), whereas they cannot withstand high pressure and most organic solvent [20], limiting their applications in synthesis of organic nanoparticles.

Manuscript received September 18, 2015; accepted August 2, 2016. Date of publication August 4, 2016; date of current version September 5, 2016. This work was supported by the Research Grants Council of Hong Kong under General Research Fund 621113. The review of this paper was arranged by associate editor SIROMA.

L. Jiang is with the Institute for Advanced Study, Hong Kong University of Science and Technology, Clear Water Bay, Hong Kong (e-mail: iasjlguo@ust.hk).

S. Yao is with the Department of Mechanical and Aerospace Engineering and Division of Biomedical Engineering, Hong Kong University of Science and Technology, Clear Water Bay, Hong Kong (e-mail: meshyao@ust.hk).

Color versions of one or more of the figures in this paper are available online at <http://ieeexplore.ieee.org>.

Digital Object Identifier 10.1109/TNANO.2016.2598242

In this work, we demonstrate an ultrafast mixing of reagents within $\sim 3 \pm 1 \mu\text{s}$ in a 3DHFF device fabricated in a silicon substrate and the use of the fabricated device for dynamic assessment of the formation of Hexaphenylsilole (HPS) nanoparticle. HPS is among the first silole derivatives that were studied when the AIE phenomenon was unearthed [21]. The HPS nanoparticles formed in the mixer have small size with narrow size distribution. We also resolved the microsecond self-assembly kinetics of HPS, indicating HPS nanoparticle formation follows the classical nucleation and growth theory.

II. 3DHFF MIXER DESIGN, FABRICATION, AND IMPLEMENTATION

A. Design

Based on our previous investigation [14], [16], [22] and the work of Gambin *et al.* [23], we designed the mixer as shown in Fig. 1(a) to achieve 3D focusing and ultrafast mixing of the sample stream. The mixer consists of a microchannel network of a deep main central channel, two pairs of shallow connection channels to achieve vertical focusing, a pair of side channels intersects with a narrow shape-optimized nozzle [14] to achieve horizontal focusing, and an exit channel with nozzle constrain. Besides, lengths of each inlet and outlet channels were carefully designed to render reasonable flow resistances for controlling liquid volumetric flow rates.

B. Fabrication

The mixer was fabricated on a silicon substrate. Two shallow connection channels were firstly photolithography patterned and etched $\sim 1.5 \pm 0.2 \mu\text{m}$ using deep reactive ion etching (DRIE), followed by patterning and etching of the main channels of $\sim 15.3 \pm 0.4 \mu\text{m}$ in depth. The liquid access holes of inlets and outlet were wet etched through the silicon substrate by Tetramethylammonium hydroxide (TMAH) with silicon oxide as the protection mask. Finally, microchannels were sealed by anodic bonding with $170 \mu\text{m}$ thick Pyrex glass and individual chips (Fig. 1(b)) were diced using a wafer cutting machine.

C. Implementation

The chip was mounted on a custom-designed holder (Fig. 1(c)), which was used for loading the sample and reagents, and connecting pressure driven lines to inlets. The volumetric flow rate in each channel was controlled by the pressure above the liquid reservoir. This pressure was regulated by LabVIEW (National Instruments) operated pressure transducers (Marsh Bellofram Type 2000, Newell, WV). In all experiments, the pressure imposed at each inlet was kept constant, and the volumetric total flow rate of the sample and other reagents was $\sim 425 \mu\text{L/h}$. Such flow condition resulted in a maximum flow velocity of $\sim 1.5 \text{ m/s}$ in the exit channel as measured below.

D. 3D Focusing Effect

We then examined the 3D focusing effect of the mixer using the laser scanning confocal microscope. Fig. 1(d) shows a two-

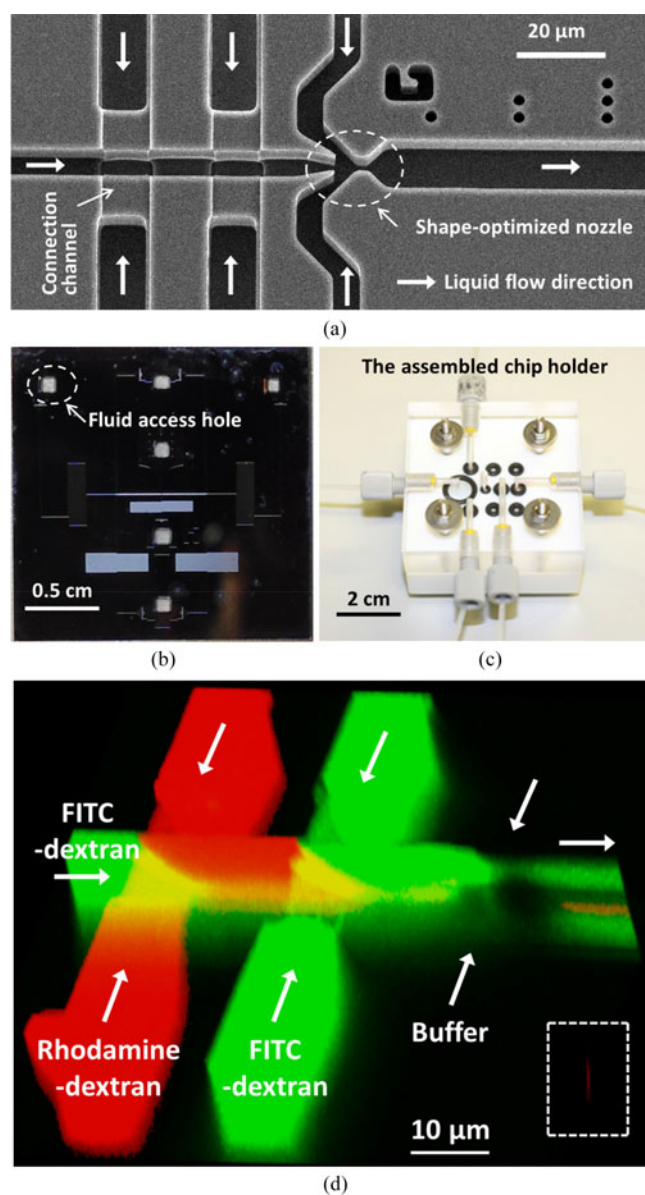


Fig. 1. (a) A SEM image shows the etched microchannels at intersection area on the silicon based mixer for achieving 3D focusing of the sample stream and ultrafast mixing of reagents. (b) An individual diced chip with a dimension of $2 \text{ cm} \times 2 \text{ cm}$. (c) The assembled chip holder ($6 \text{ cm} \times 6 \text{ cm}$) for liquid sample loading, products collection, and driven pressure access. (d) A two-color fluorescence confocal image of liquid flow in the mixer clearly shows the vertical and horizontal focusing effect. The cross section view of the exit channel (the inset image with white dashed lines) shows the isolated sample stream (red color) with nearly uniform width in the center of the channel.

color fluorescence imaging of the liquid flow in the mixer. The Rhodamine-dextran labeled sample streams (red color) originated from the first pair of connection channels was vertically focused by FITC-dextran labeled streams (green color), forming a vertically sandwiched stream in the main central channel. Then, the sandwiched stream was laterally focused by two phosphate buffer (PB) streams from two side channels, resulting in a 3D focused narrow jet of the Rhodamine-dextran stream. The cross-sectional image of the exit channel (inset of Fig. 1(d)) shows that the sample stream is located in the center of the channel and isolated from all the channel walls (indicated by white

dashed lines). Importantly, the 3D focused stream has a uniform width, which ensures uniform mixing across the stream.

III. COMPUTATIONAL AND EXPERIMENTAL CHARACTERIZATION OF THE MIXER

A. Computational Fluid Dynamics (CFD) Simulations

To quantify the fluid flow and mixing dynamics of 3D focused stream in the micromixer, we performed CFD simulations using a commercial finite element code, COMSOL multiphysics 4.1. Fluid flow inside microchannel is governed by the incompressible steady-state Navier-Stokes equations, represented by the single phase *laminar flow model* in the simulation, and the mixing is governed by the steady-state convective-diffusion equation, coupled into the simulation by the *transport of diluted species model*:

$$\nabla \cdot \vec{V} = 0 \quad (1)$$

$$\rho(\vec{V} \cdot \nabla)\vec{V} = -\nabla P + \mu\nabla^2\vec{V} \quad (2)$$

$$\vec{V} \cdot \nabla C = D\nabla^2 C \quad (3)$$

where \vec{V} is the flow velocity, ρ is the fluid density, P is the pressure, μ is the fluid dynamic viscosity, C is the concentration of a sample, and D is the diffusion coefficient of the sample in water. Together with boundary and initial conditions, equations (1)–(3) provide a numerical way to calculate the flow velocity and concentration fields.

A symmetric 2D model of the micromixer was created to simulate the fluid flow in the micromixer as illustrated in Fig. 2(a) (together showing meshing elements). The model contains two inlet boundary, one outlet boundary, one symmetric boundary, and the surface wall boundary. The two flow inlets were set as laminar inflows with the average flow velocity of 0.056 m/s at the central inlet and 1.03 m/s at the side inlet. The flow outlet was set as laminar outflows with exit pressure of 0 Pa. In the mesh setting, the model was separated into two regions: the mixing region and non-mixing region. The mixing region is the region where two streams are intersected and mixing takes place. In the mixing region, extremely fine triangular meshes with maximum element size of 10 nm was applied (the region with denser mesh elements in Fig. 2(a)). Other than the mixing region, triangular meshes were set with maximum element size of 0.2 μm .

To quantify the fluid velocity in the microfluidic device, we traced 10 streamlines from the focused central stream in our 2D model. Fig. 2(b) shows the result of simulated flow velocity field. Color map from dark blue to dark red represents the magnitude of flow velocity from 0 to 5.5 m/s. Co-plotted white lines are 10 traced streamlines. Fig. 2(c) shows the average flow velocity on the 10 streamlines along the x axis. The results show that the maximum flow velocity is ~ 5.5 m/s and ~ 1.5 m/s at the constriction nozzle and in the exit channel, respectively.

B. The Flow Circuit Model

We utilizes compressed gas (typically on the order of tens of psi) to drive fluid flow inside the microchannels. Accord-

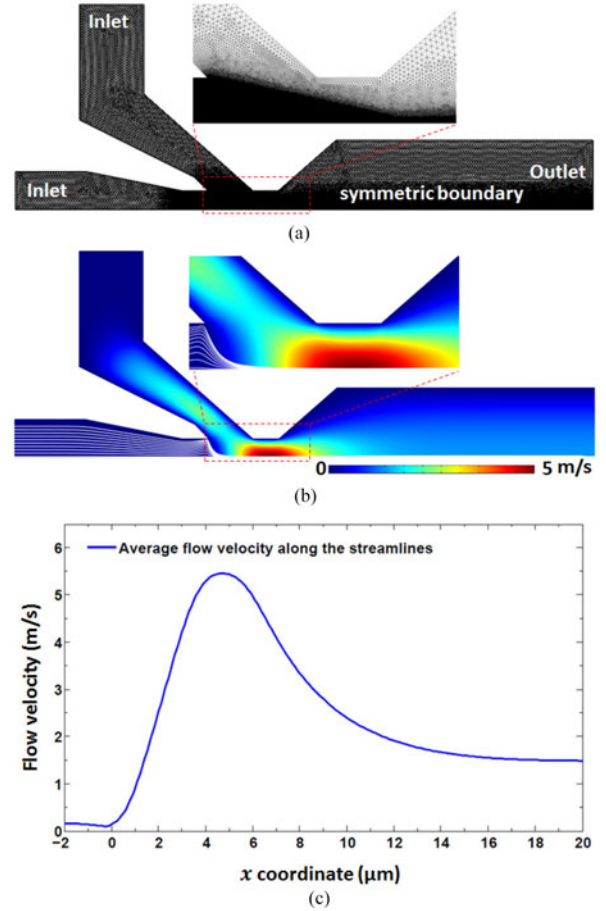


Fig. 2. (a) A schematic of the symmetric 2D model of the mixer with meshing elements. An extremely fine triangular mesh with maximum element size of 10 nm was applied at denser element area. An extra fine triangular mesh with maximum element size of 0.2 μm was applied at the other area. The model has two inlets, one outlet, a symmetric boundary, and the other surface walls. (b) Color map shows the simulated flow velocity field. The maximum flow velocity located at the center of the exit constrained nozzle is ~ 5.5 m/s. The maximum flow velocity in the exit channel is ~ 1.5 m/s. Co-plotted white lines are 10 streamlines. (c) The simulation result of the averaged flow velocity along 10 streamlines.

ing to the Navier-Stokes equations (1) and (2), the volumetric flow rates of each inlet can be theoretically calculated when the inlets pressures and the geometries of microchannel networks are given. For microchannels with constant rectangular cross section, the driving pressure drop ΔP is linearly correlated with the microchannel length L and the volumetric flow rate Q [24]:

$$\Delta P = Q \cdot R_{\text{hyd}} \quad (4)$$

$$R_{\text{hyd}} = \frac{12\eta L}{1 - 0.63(h/w)} \frac{1}{h^3 w} \quad (5)$$

where R_{hyd} is called the hydraulic resistance, η is the fluid viscosity, h is the channel height, and w is the channel width. Based on the design of the microchannel network and the equations (4) and (5), a flow resistance circuit model can be created to estimate the volumetric flow rate inside the mixer as shown in Fig. 3(a). And the relationships between the input

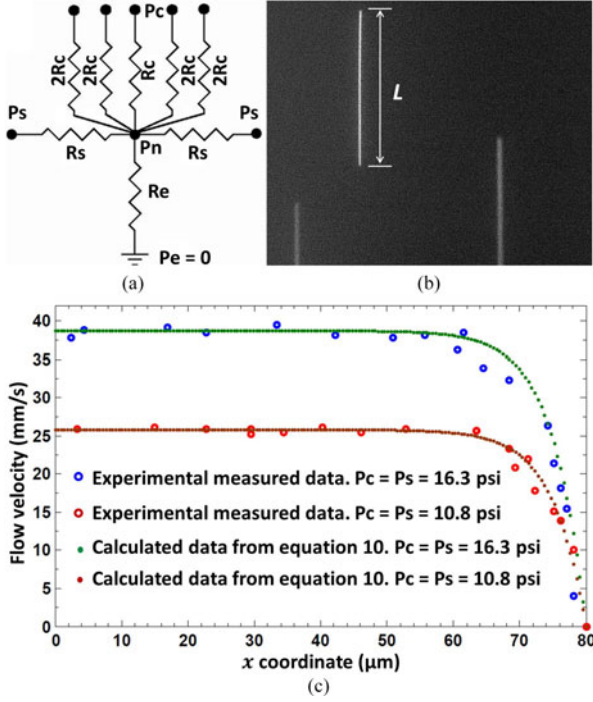


Fig. 3. (a) A schematic shows the flow resistance circuit model for theoretically calculating the volumetric flow rates in the designed 3D focusing mixer. (b) A demonstration of a captured trajectory of a fluorescent microparticle. (c) The comparison of the experimentally measured flow velocities (colored circles) and the theoretically calculated flow velocities (colored dots) shows good agreement, indicating the accuracy of the circuit model for estimating the flow velocities in the mixer.

pressures and volumetric flow rates are:

$$Q_c = \frac{P_c}{R_{ct}} - \frac{P_c \frac{R_s}{R_{ct}} + 2P_s}{\frac{R_{ct}R_s}{R_e} + R_s + 2R_{ct}} \quad (6)$$

$$Q_s = \frac{P_s}{R_s} - \frac{P_c + 2P_s \frac{R_{ct}}{R_s}}{\frac{R_{ct}R_s}{R_e} + R_s + 2R_{ct}} \quad (7)$$

where Q_c is the total volumetric flow rates of center channels, Q_s is the volumetric flow rate of individual side channel, P_c is the center input pressure, P_s is the side input pressure, $R_{ct} = R_c/3$ is the combined hydraulic resistance of five center channels, R_s is the side channel hydraulic resistance, and R_e is the exit channel hydraulic resistance.

C. The Measurement of Fluid Flow Velocity

The flow circuit model introduced above allows us to estimate the volumetric flow rate in each inlet channel at fixed input pressures. To verify this model, we utilized the fluorescent microparticle trajectory imaging technique to measure the flow velocities in the mid-plane of a side channel where the channel width is $160 \mu\text{m}$. The technique uses a high sensitive CCD camera (Q-imaging) equipped on an epifluorescence microscopy (Nikon) to capture the trajectories of flowing fluorescent polystyrene microparticles ($0.5 \mu\text{m}$ diameter) inside the mixer. And the flow velocity of the microparticle at specific

channel location can be calculated as:

$$V = L/t \quad (8)$$

where L is the captured trajectory length of a fluorescent microparticle shown in the image and t is the exposure time of the image.

Fig. 3(b) illustrates a captured trajectory of a microparticle as indicated by L using the developed fluorescent microparticle trajectory imaging technique. The length of this trajectory can be well measured in pixels and the pixel size was precisely calculated from the scale plate fabricated on the device. Therefore, the flow velocity of this captured microparticle can be obtained from equation (8). On the other hand, by using the calculated volumetric flow rate from the flow circuit model at given input pressures as the initial flow condition, the flow velocity in the side channel also can be obtained by the CFD simulations. The experimentally measured flow velocities on the mid-plane of the side channel were compared with the simulated flow velocities at two different input pressures, and the results are shown in Fig. 3(c). Clearly, the experimental data matched very well with the simulation data at both flow conditions. Those results suggest that our flow circuit model provides accurately prediction of the volumetric flow rate inside the micromixer. For instance, at the input pressures of $P_c = P_s = 16.3 \text{ psi}$, the maximum flow velocity at the center of the exit channel is indeed $\sim 1.5 \text{ m/s}$.

D. Mixing Time Characterization by Dye Quenching Experiments and Simulations

We further characterized the mixing time of the mixer using the dye quenching technique [13]. In dye quenching experiments, the FITC-dextran labeled sample stream was 3D focused and the PB buffer with the absent or present of fluorophore quencher, the iodide ion $[I^-]$ at a concentration of 0.2 M , was pumped into the two side channels. Confocal fluorescent images were taken as shown in Fig. 4(a). Both images illustrate that the fluorescent dye stream was tightly focused to a narrow jet with a width of $< 200 \text{ nm}$. As the diffusion of iodide ions (diffusivity of $2 \times 10^{-9} \text{ m}^2/\text{s}$) is ~ 5 times faster than that of dextran 10K labeled FITC molecules (diffusivity of $1 \times 10^{-10} \text{ m}^2/\text{s}$), mixing is rapidly accomplished by the iodide ions diffusing across the focused stream and quenching the fluorescent intensity of FITC-dextran molecules in the focused central stream. Fig. 4(b) shows the extracted fluorescent intensities of the unquenched (blue dots) and quenched (green dots) samples along the focused jet.

We also simulated the diffusion of iodide ion $[I^-]$ in the micromixer using the CFD model presented above. For comparison, we set the mixing condition in the CFD simulation being consistent with that in dye quenching experiments above. We set the iodide ions flowing from the side streams and diffusing into the focused central stream. Followed the suggestion from Hertzog *et al.* [13] and Park *et al.* [25], we traced 10 streamlines from the focused central stream, and to define the mixing time t_i of each streamline in the focused jet, of which the clock starts when the concentration of $[I^-]$ along the streamline has increased to the 1% of the concentration in the side stream, and the average mixing time $\langle t \rangle$ at x location is calculated by summing and

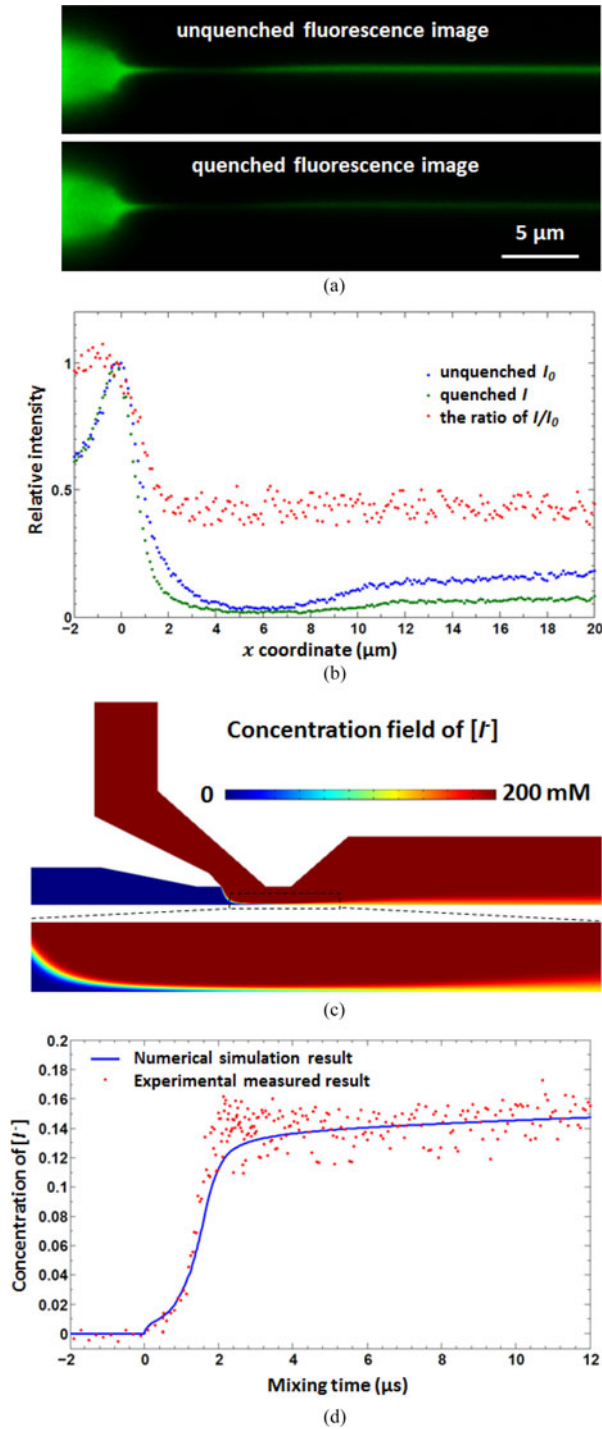


Fig. 4. Simulation and the dye quenching experiments demonstrate the mixer has a mixing time of $\sim 3 \pm 1 \mu\text{s}$. (a) Fluorescence confocal images of 3D focused stream when FITC-dextran fluorescence is unquenched (up) and quenched (low) upon mixing with iodide ions. (b) The plot of extracted unquenched (blue dots) and quenched (green dots) fluorescence intensities along the focused stream. The ratio of the two intensities (red dots) indicates the mixing of dye molecules with iodide ions in the space domain. (c) Color map shows the simulated $[I^-]$ concentration field. $[I^-]$ ions originally come from the side channel and diffuse into the center of the exit channel. (d) The intensity ratio was converted to the concentration of the iodide ions $[I^-]$ based on the Stern-Volmer equation, and the spatial coordinates were converted to the time coordinates based on the flow field in the exit channel obtained in Fig. 3(a), indicating the mixing time of $\sim 3 \pm 1 \mu\text{s}$. Co-plotted blue line is the CFD simulation result of mixing time in (c).

averaging the contribution of mixing times from all streamlines:

$$t_i(x) = \int_{x_0, c=0.01c_0}^x \frac{dx}{u_i(x)} \quad (9)$$

$$\langle t(x) \rangle = \frac{\sum_i t_i(x) w_i(x)}{\sum_i w_i(x)} \quad (10)$$

and standard deviation of the mixing time, which represents the mixing uniformity across the x location, is defined as:

$$\sigma(x) = \sqrt{\frac{\sum_i (t_i(x) - \langle t(x) \rangle)^2 w_i(x)}{\sum_i w_i(x)}} \quad (t_i > 0) \quad (11)$$

where u_i is the x component of the flow velocity in the i th streamline, w_i is the width of the i th streamline, and C_0 is the initial concentration of the iodide ion. All the simulated data were analyzed using customer-built programs in MATLAB. Fig. 4(c) shows the simulated concentration field with color map representing $[I^-]$ concentration from 0 to 0.2 M. The results show that the $[I^-]$ concentration among the streamlines is rapidly approaching to the bulk concentration at downstream after mixing is initialized. Mixing time and mixing uniformity (the standard deviation of the mixing time) as defined in the equations (10) and (11) are two crucial parameters that quantify the mixing performance of a micromixer. The mixing time directly reveals the time that the micromixer is needed to trigger a reaction, and the mixing uniformity directly influences the deviation of the reaction kinetics. Our designed and fabricated micromixer can achieve ultrafast mixing within a few microseconds while minimize the mixing time deviation (below 10% of the mixing time).

To obtain the concentration of the quencher $[I^-]$ along the jet, we further performed a calibration of the Stern-Volmer equation:

$$I_0/I = 1 + K_{SV} [I^-] \quad (12)$$

where I_0 and I are fluorescence intensities of the unquenched and quenched samples; $[I^-]$ is the concentration of the quencher, and K_{SV} is the Stern-Volmer constant. In our experiments, K_{SV} has a value of 10.5, which was obtained from the calibration of fluorescent intensities at different concentrations of the iodine ions $[I^-]$.

Using the Stern-Volmer equation, we converted the intensity ratio (red dots in Fig. 4(b)) to the iodine concentration as shown in Fig. 4(d) (red dots). The spatial coordinates along the focused jet were converted to the time coordinates using the flow field obtained from the simulation and experimental characterization presented above. Co-plotted solid blue line is the numerical simulation results of $[I^-]$ diffusing into the focused stream in the time domain. Both experimental and simulation results show that the mixing is essentially completed within $\sim 3 \pm 1 \mu\text{s}$.

IV. APPLICATION OF THE MIXER FOR DYNAMIC ASSESSMENT OF HPS NANOPARTICLE FORMATION

A. HPS Nanoparticle Formation in the Mixer

HPS molecules (inset of Fig. 5 shows the chemical structure of HPS) are well dissolved in many organic solvents, but

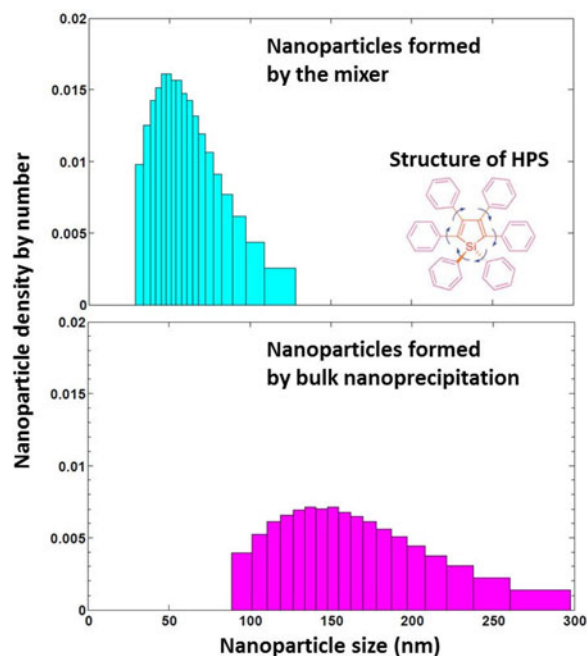


Fig. 5. Results of the DLS measurement show the nanoparticles formed by the mixer (up) has a relatively smaller size and narrower size distribution, compared to those formed by bulk nanoprecipitation (below) at the identical final HPS concentration and solvent condition. The inset shows the chemical structure of HPS molecule.

they tend to self-assemble into nanoparticles when mixing with water. The force that drives HPS molecules to self-assemble is the strong intermolecular hydrophobic interactions due to the six aromatic rings of a molecule. Chen *et al.* [21] demonstrated that HPS nanoparticles were formed when the addition of water molecules occupied a volume fraction larger than 0.5. In this work, we applied the micromixer to investigate the formation of HPS nanoparticle. TEM images showed that the formed HPS nanoparticles have perfect spherical shape [26]. In our experiments, the sample solution of HPS dissolved in pure Dimethyl sulfoxide (DMSO) solvent at a concentration of 3 mM was pumped into the first pair of shallow connecting channels (e.g. the two channels contain red streams in Fig. 1(d)). The pure DMSO solvent was pumped into the deep main central channel and the second pair of shallow connecting channels (e.g. the three channels contain green streams in Fig. 1(d)). And pure water was pumped into two side channels (e.g. the two buffer streams in the Fig. 1(d)). The HPS stream was first vertically focused by pure DMSO streams and then horizontally focused by pure water stream to achieve 3D focusing. The formed HPS nanoparticles in the mixer were collected at the exit channel for further analysis. We also used the bulk nanoprecipitation method to form HPS nanoparticles by dropping a small amount of HPS stock solution into water and bulk vortex mixing. In both experiments, the final HPS concentration ($\sim 10 \mu\text{M}$) and DMSO solvent volume fraction (3%) were kept identical for comparison. Fig. 5 shows the nanoparticle size distribution measured by DLS. Nanoparticles formed by bulk nanoprecipitation (magenta bars) have a wide size range, with diameters of ~ 80 to

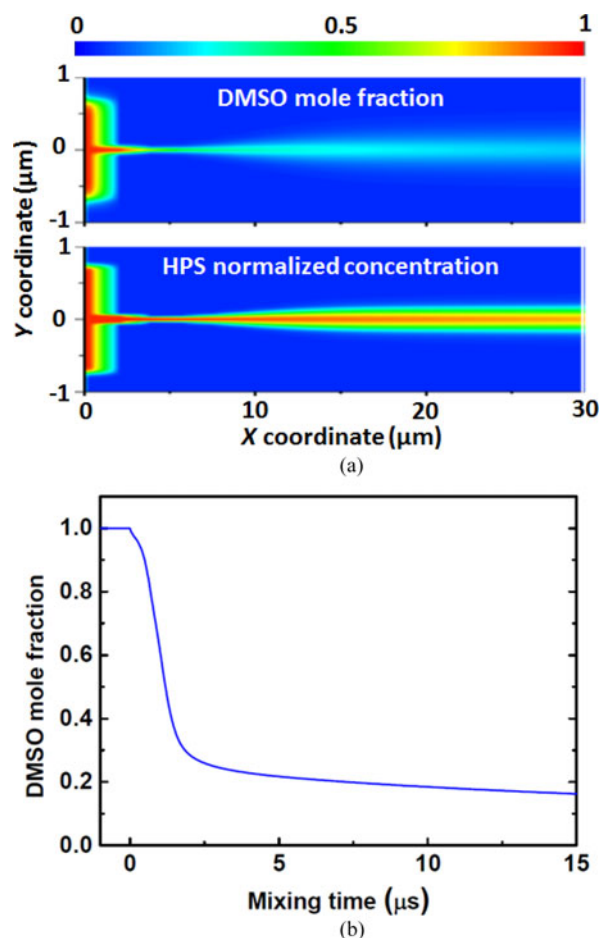


Fig. 6. CFD simulating the depletion of DMSO solvent and the diffusion of HPS in the mixer. (a) Enlarged focused streams show the diffusion of DMSO and HPS molecules. The HPS molecules were confined in the focused central stream at high concentrations whereas the DMSO molecules rapidly diffuse out of the focused central stream in the lateral direction resulting a jump decrease of its mole fraction. (b) Detailed plot of the depletion of DMSO mole fraction along streamlines defined in Fig. 2(b). The DMSO mole fraction depletes rapidly to a value of ~ 0.2 within $\sim 3 \mu\text{s}$.

300 nm. However, the nanoparticles formed in the mixer (cyan bars) shows a much smaller size and relatively narrower size distribution, with diameters of ~ 30 to 130 nm. The more controllable synthesis of nanoparticle by the mixer is likely due to the rapid mixing and the relatively homogeneous environment created in the 3D focused stream.

To better understand the mechanism of nanoparticle precipitation in the mixer, we performed CFD simulation to capture the DMSO solvent depletion and the diffusion of HPS molecules in the mixer using the CFD model presented above. In the simulation, the fluid density, dynamic viscosity, and diffusion coefficient in equations (2) and (3) were a function of the DMSO molar concentration and were expressed by a fourth-order polynomial fitting density data, viscosity data, and diffusion coefficient data as reported in literatures [27], [28]. The diffusion coefficient of HPS molecules was calculated based on the Stokes–Einstein equation with a diffusive radius of 6.3 \AA . Fig. 6(a) shows the simulation results. Both DMSO and HPS laterally diffuse out

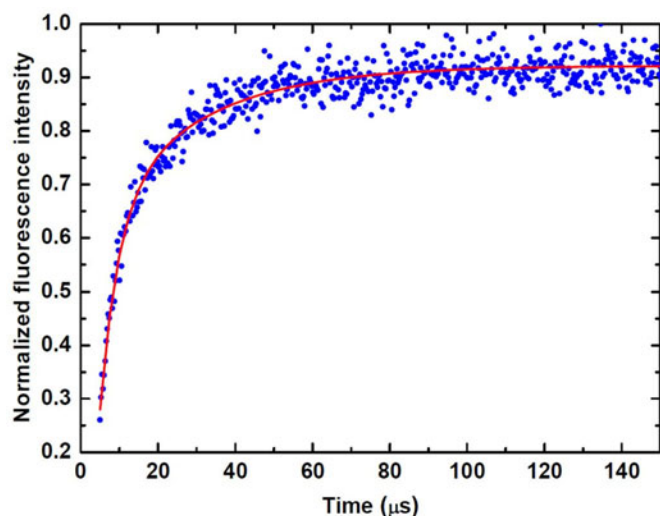


Fig. 7. The microsecond kinetics of HPS nanoparticle formation measured in the mixer. The solid red line is the two-exponential growth model fitting of the experimental data. The fitted two growth rates, $0.21 \mu\text{s}^{-1}$ and $0.039 \mu\text{s}^{-1}$, indicate that two distinct steps are involved in the HPS nanoparticle formation. The measured kinetics clearly demonstrates the capability of the mixer for studies of molecular self-assembly kinetics on the microsecond timescale.

of the focused stream in the mixer. Clearly, the HPS molecules were confined in the focused central stream and remained a high concentration whereas the DMSO solvent rapidly depletes in mole fraction (ratio of DMSO molar concentration to the total DMSO and water molar concentrations) along the focused central stream. Detailed plots of DMSO mole fraction (Fig. 6(b)) indicate that the DMSO mole fraction depletes rapidly to a value of ~ 0.2 within $\sim 3 \mu\text{s}$ whereas the HPS maintains a high concentration (80–90% of its initial concentration) in the focused stream. Consequently, this rapid depletion of the DMSO in the focused stream provides a homogenous solvent environment to trigger HPS molecules self-assembling into nanoparticles.

B. Microsecond Self-Assembly of HPS Molecules

To understand the molecular mechanism of the HPS nanoparticle formation, we further measured the kinetics of HPS molecular self-assembly. HPS is an AIE fluorophore [21], which is non-emissive in free molecule state but highly luminescent when they are forming nanoparticles in water. Hence, by capturing the fluorescence on the trajectory of the 3D focused jet under the laser scanning confocal microscope, the kinetics of the HPS nanoparticle formation can be exactly followed in the time domain. The measured kinetics (Fig. 7) can be well fitted by the two-exponential growth model with growth rate of $0.21 \mu\text{s}^{-1}$ and $0.039 \mu\text{s}^{-1}$, indicating that two distinct steps are involved in the HPS nanoparticle formation. These results suggest that the formation of the HPS nanoparticles very likely obeys the classical nucleation and growth theory [29].

Rapid mixing is key in obtaining smaller and uniform size of HPS nanoparticles as demonstrated in Fig. 5. When the DMSO stream carrying HPS molecules flow into the mixer, fast mixing of DMSO stream with water streams is critical to provide

a homogenous solvent environment for HPS nuclei formation and growth (Fig. 7). Hence, we speculate that by controlling the mixing condition in the mixer (e.g. changing the total flow rates and flow rate ratios of HPS sample streams, DMSO streams, and pure water streams), we can achieve controllable formation of HPS nanoparticles with tunable size. In addition, the initial concentration of HPS dissolved in DMSO solvent is also a critical parameter for controlling HPS nanoparticle nucleation and growth processes. According to the classical nucleation and growth theory [29], the supersaturation ratio, which is the ratio of the concentration of a solute in the solution to the solubility of the solute, determines the nucleation rate and growth rate during nanoparticle formation. Hence, the initial concentration of HPS in the solution governs the nucleus formation and controls the growth of HPS nuclei.

V. CONCLUSION

In conclusion, we report the design, fabrication, and characterization of a silicon based mixer with 3D focusing. The 3D focused sample stream was isolated from the surface walls by the sheath flow in both vertical and horizontal directions, thereby preventing surface sticking and channel clogging problems. The sample in the focused stream was rapidly mixed with other reagents within $\sim 3 \pm 1 \mu\text{s}$. The ultrafast mixing was confirmed by CFD simulations and dye quenching experiments. We demonstrated the application of the mixer for dynamic assessment of the HPS nanoparticle formation. The nanoparticles formed in the mixer showed smaller size with narrower size distribution, compared to those formed by bulk nanoprecipitation. Moreover, the measured formation kinetics suggests that two distinct steps are involved in the HPS nanoparticle formation. In principle, the mixer is applicable for dynamically assessing the formation of a wide range of nanomaterials.

ACKNOWLEDGMENT

The authors would like to thank the group of Prof. B. Tang, the group of Prof. B. Huang, the Nanoelectronic Fabrication Facility, the Biosciences Central Research Facility, and the Advanced Engineering Material Facility at HKUST for their technique support.

REFERENCES

- [1] R. Singh and J. W. Lillard Jr, "Nanoparticle-based targeted drug delivery," *Exp. Mol. Pathol.*, vol. 86, pp. 215–223, 2008.
- [2] P. Sharma, S. Brown, G. Walter, S. Santra, and B. Moudgil, "Nanoparticles for bioimaging," *Adv. Colloid. Interface. Sci.*, vol. 123–126, pp. 471–485, 2006.
- [3] A. N. Shipway, E. Katz, and I. Willner, "Nanoparticle arrays on surfaces for electronic, optical, and sensor applications," *ChemPhysChem*, vol. 1, pp. 18–52, 2000.
- [4] Y. Hong, J. W. Y. Lam, and B. Z. Tang, "Aggregation-induced emission: Phenomenon, mechanism and applications," *Chem. Commun.*, vol. 29, pp. 4332–4353, 2009.
- [5] K. Li *et al.*, "Photostable fluorescent organic dots with aggregation-induced emission (AIE dots) for noninvasive long-term cell tracing," *Sci. Rep.*, vol. 3, Art. no. 1150 (2013).
- [6] S. Zhang, "Fabrication of novel biomaterials through molecular self-assembly," *Nat. Biotechnol.*, vol. 21, pp. 1171–1178, 2003.

- [7] J. Rodriguez-Hernandes, F. Checot, Y. Gnanou, and S. Lecommandoux, "Toward 'smart' nano-objects by self-assembly of block copolymers in solution," *Prog. Polym. Sci.*, vol. 30, pp. 691–724, 2005.
- [8] L. Zang, Y. Che, and J. S. Moore, "One-dimensional self-assembly of planar π -conjugated molecules: Adaptable building blocks for organic nanodevices," *Acc. Chem. Res.*, vol. 41, pp. 1596–1608, 2008.
- [9] F. Alexis, E. Pridgen, L. K. Molnar, and O. C. Farokhzad, "Factors affecting the clearance and biodistribution of polymeric nanoparticles," *Mol. Pharmaceutics*, vol. 5, pp. 505–515, 2008.
- [10] Y. Song, J. Hormes, and C. S. S. R. Kumar, "Microfluidic synthesis of nanomaterials," *Small*, vol. 4, pp. 698–711, 2008.
- [11] L. Capretto, D. Carugo, S. Mazzitelli, C. Nastruzzi, and X. Zhang, "Microfluidic and lab-on-a-chip preparation routes for organic nanoparticles and vesicular systems for nanomedicine applications," *Adv. Drug Del. Rev.*, vol. 65, pp. 1496–1532, 2013.
- [12] G. Lee, C. Chang, S. Huang, and R. Yang, "The hydrodynamic focusing effect inside rectangular microchannels," *J. Micromech. Microeng.*, vol. 16, pp. 1024–1032, 2006.
- [13] D. E. Hertzog *et al.*, "Femtomole mixer for microsecond kinetic studies of protein folding," *Anal. Chem.*, vol. 76, pp. 7169–7178, 2004.
- [14] S. Yao and O. Bakajin, "Improvements in mixing time and mixing uniformity in devices designed for studies of protein folding kinetics," *Anal. Chem.*, vol. 79, pp. 5753–5759, 2007.
- [15] M. Rhee, P. M. Valencia, M. Rodriguez, R. Langer, O. C. Farokhzad, and R. Karnik, "Synthesis of size-tunable polymeric nanoparticles enabled by 3D hydrodynamic flow focusing in single-layer microchannels," *Adv. Mater.*, vol. 23, pp. H79–H83, 2011.
- [16] L. Jiang, W. Wang, Y. Chau, and S. Yao, "Controllable formation of aromatic nanoparticles in a three-dimensional hydrodynamic flow focusing microfluidic device," *RSC Adv.*, vol. 3, pp. 17762–17769, 2013.
- [17] M. Lu, Y. P. Ho, C. L. Grigsby, A. A. Nawaz, K. W. Leong, and T. J. Huang, "Three-dimensional hydrodynamic focusing method for polyplex synthesis," *ACS Nano*, vol. 8, pp. 332–339, 2014.
- [18] X. Mao, J. R. Waldeisen, and T. J. Huang, "Microfluidic drifting—implementing three-dimensional hydrodynamic focusing with a single-layer planar microfluidic device," *Lab Chip*, vol. 7, pp. 1260–1262, 2007.
- [19] X. Mao, S. S. Lin, C. Dong, and T. J. Huang, "Single-layer planar on-chip flow cytometer using microfluidic drifting based three-dimensional (3D) hydrodynamic focusing," *Lab Chip*, vol. 9, pp. 1583–1589, 2009.
- [20] J. Ng Lee, C. Park, and G. M. Whitesides, "Solvent compatibility of poly(dimethylsiloxane)-based microfluidic devices," *Anal. Chem.*, vol. 75, pp. 6544–6554, 2003.
- [21] J. Chen, C. C. W. Law, J. W. Y. Lam, Y. Dong, S. M. F. Lo, I. D. Williams, D. Zhu, and B. Tang, "Synthesis, light emission, nanoaggregation, and restricted intramolecular rotation of 1,1-substituted 2,3,4,5-tetraphenylsiloles," *Chem. Mater.*, vol. 15, pp. 1535–1546, 2003.
- [22] L. Jiang, Y. Zeng, Q. Sun, Y. Sun, Z. Guo, J. Y. Qu, and S. Yao, "Microsecond protein folding events revealed by time-resolved fluorescence resonance energy transfer in a microfluidic mixer," *Anal. Chem.*, vol. 87, pp. 5589–5595, 2015.
- [23] Y. Gambin, C. Simonnet, V. vanDelinder, A. Deniz, and A. Groisman, "Ultrafast microfluidic mixer with three-dimensional flow focusing for studies of biochemical kinetics," *Lab Chip*, vol. 10, pp. 598–609, 2010.
- [24] H. Bruus, *Theoretical microfluidics*, vol. 18, New York, NY, USA: Oxford Univ. Press, 2007.
- [25] H. Y. Park *et al.*, "Achieving uniform mixing in a microfluidic device: Hydrodynamic focusing prior to mixing," *Anal. Chem.*, vol. 78, pp. 4465–4473, 2006.
- [26] G. He, H. Peng, T. Liu, M. Yang, Y. Zhang, and U. Fang, "A novel picric acid film sensor via combination of the surface enrichment effect of chitosan films and the aggregation-induced emission effect of siloles," *J. Mater. Chem.*, vol. 19, pp. 7347–7353, 2009.
- [27] J. Catalan, C. Diaz, and F. Garcia-Blanco, "Characterization of binary solvent mixtures of DMSO with water and other cosolvents," *J. Org. Chem.*, vol. 66, pp. 5846–5852, 2001.
- [28] I. A. Borin and M. S. Skaf, "Molecular association between water and dimethyl sulfoxide in solution: A molecular dynamics simulation study," *J. Chem. Phys.*, vol. 110, pp. 6412–6420, 1999.
- [29] D. Kashchiev and G. M. vanRosmalen, "Review: Nucleation in solutions revisited," *Cryst. Res. Technol.*, vol. 38, pp. 555–574, 2003.



Liguojiang received the B.Sc. degree from the Department of Modern Mechanics, University of Science and Technology of China, Anhui, China, in 2009, and the Ph.D. degree in bioengineering from the Hong Kong University of Science and Technology (HKUST), Hong Kong, China, in 2013. He is currently a Postdoctoral Fellow in HKUST Institute for Advanced Study. His research interests include design of ultrafast microfluidic mixer for study of the biological system, fluorescence spectroscopy study of a single molecule, protein amyloid fibrillation, protein crystallization, controllable synthesis of nanomaterials, and microfluidic single-cell genomics.



Shuhuai Yao received the B.Sc. degree in engineering mechanics from Tsinghua University, Beijing, China, in 2000, and the M.S. and Ph.D. degrees in mechanical engineering from Stanford University, Stanford, CA, USA, in 2001 and 2005, respectively. Before joining the Hong Kong University of Science and Technology, Hong Kong, China, she was a Postdoctoral Fellow at the Lawrence Livermore National Laboratory. She is currently an Associate Professor with the Department of Mechanical and Aerospace Engineering, Hong Kong University of Science and Technology. Her research interest lies in understanding of micro-/nanoscale fluid dynamics and heat transfer, interfacial surface science and transport phenomena, and applying new technologies from fundamental studies to electronics cooling and bioanalytical devices.